ELSEVIER

Signal Processing: *Image Communication* 16 (2001) 657–668

SIGNAL PROCESSING:
IMAGE
COMMUNICATION

www.elsevier.nl/locate/image

Adaptive 3-D median filtering for restoration of an image sequence corrupted by impulse noise

Jun-Seon Kim[1], Hyun Wook Park*

Department of Electrical Engineering, Korea Advanced Institute of Science and Technology, 373-1 Kusung-dong, Yusong-gu, Taejon 305-701, South Korea

Abstract

An adaptive 3-D median filtering, which achieves optimal image quality as well as fast computing time, is proposed to remove the impulse noise from a highly corrupted image sequence. The proposed algorithm is compared with the widely used impulse noise removal algorithms with respect to the peak signal-to-noise ratio and the number of computations. The proposed algorithm preserves the image details which are not expected to be corrupted by impulse noise so that the number of computations can be minimized. It has good restoration performance whether the number of pixels corrupted by impulse noise is large or small. In the proposed algorithm, the impulse noise ratio, which is the ratio of the number of pixels corrupted by impulse noise to the total number of pixels, is estimated, and the restoration filtering is adaptively applied based on the estimated impulse noise ratio. © 2001 Elsevier Science B.V. All rights reserved.

Keywords: Adaptive filter; Impulse noise; 3-D median filter; Image restoration

1. Introduction

In the early development of signal and image processing, linear filters were the primary tools for image enhancement and restoration [4]. Because the linear filters were mathematically simple and had several desirable properties, it was easy to design and use. Moreover, the linear filters offer satisfactory performance in many applications. However, the linear filters are not efficient when the noise is not additive Gaussian or when the system is nonlinear. In addition, various criteria, e.g., the maximum entropy criterion, lead to nonlinear solutions [8].

Images are often corrupted by impulse noise due to noisy sensors or channel transmission errors. Several impulse noise removal techniques have been developed to suppress the impulse noise while preserving the image details [1,6]. Nonlinear techniques have been found to provide better results for impulse noise removal in comparison with linear methods [8,10]. In general, median filters, weighted median filters, and order statistic filters have reduced the impulse noise well.

In this paper, 3-D image data refer to temporal sequences of 2-D spatial images. The proposed adaptive 3-D median filtering restores a 3-D image which has been corrupted by impulse noise. The proposed algorithm employs such signal adaptive techniques as a *noise rate switch* in the spatial domain and a 1-D/3-D *switch* in the time domain in order to improve the peak signal-to-noise ratio

[1] Now with LG Electronics Co., Seoul, South Korea

* Corresponding author.

E-mail address: hwpark@athena.kaist.ac.kr (H.W. Park).

PII: S0923-5965(00)00043-6

(PSNR) and reduce the number of computations.

This paper is organized as follows. Section 2 presents the definition of the impulse noise, which is considered in this paper. Section 3 describes the proposed algorithm to reduce the impulse noise. In Section 4, the proposed algorithm is evaluated and compared with conventional nonlinear impulse noise removal techniques with respect to the PSNR and the number of computations. The comparison study of the nonrecursive and the recursive implementations is described in Section 5. Finally, conclusions are given in Section 6.

2. Impulse noise (salt-pepper noise)

Impulse or salt-pepper noise can occur due to a random bit error in a communication channel [9]. It appears as black and/or white impulses on the image. Its source is usually man-made or atmospheric noise which appears as the impulse noise. The corrupted image from the impulse noise is defined as follows:

$$n(k,j) = \begin{cases} z(k,j) & \text{with probability } p, \\ i(k,j) & \text{with probability } (1-p), \end{cases} \tag{1}$$

where $z(k,j)$ denotes an impulse and $i(k,j)$ denotes the original image intensity at (k,j) [8].

For computer simulations, a corrupted image is generated which has fixed-value impulse noise of 0 or 255 with equal probabilities or random value impulse noise with a uniform distribution from 0 to 255, where each pixel has an 8-bit resolution [1]. The impulse noise ratio is the ratio between the number of pixels corrupted by the impulse noise and the total number of pixels in the image. A different impulse noise ratio is applied to each image frame of an image sequence in the simulation, as shown in Fig. 1.

In this paper, four image sequences are used for simulation: the Akiyo, the Mother & Daughter, the News, and the Foreman sequences. Each sequence has 300 image frames. Fig. 2 shows the PSNRs of the Akiyo sequence corrupted by the impulse noise. The other image sequences are also corrupted by the impulse noise in the same way as the Akiyo sequence.

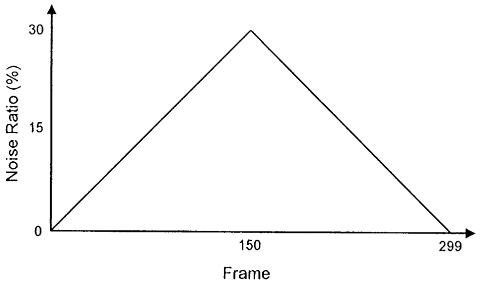

Fig. 1. The impulse noise ratio of each frame in the test image sequence. The impulse noise ratio is defined as the ratio between the number of corrupted pixels and the total number of pixels in a frame.

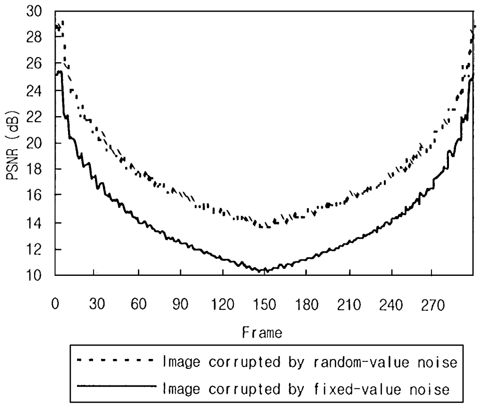

Fig. 2. The PSNR of the Akiyo sequence corrupted by the random-value and fixed-value impulse noise. Each frame is corrupted by impulse noise with a different noise ratio, as shown in Fig. 1.

3. The proposed impulse noise removal algorithm

Three-dimensional median-related operations have been successfully developed to reduce the impulse noise [7]. Since most image sequences have high correlation between consecutive frames, the 3-D filtering is more efficient than the 2-D filtering in terms on PSNR. However, the 3-D filtering

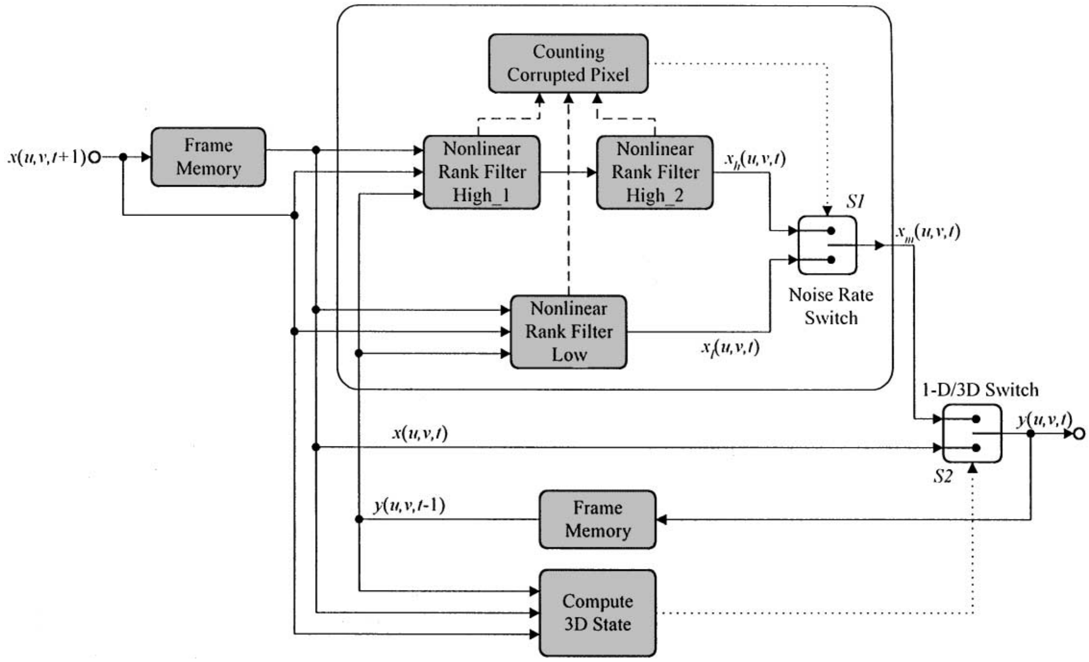

Fig. 3. The block diagram of the proposed adaptive 3-D median filtering algorithm.

requires relatively large amount of computations. The proposed impulse noise removal algorithm is an adaptive 3-D filtering whose block diagram is shown in Fig. 3. The proposed adaptive 3-D filtering has high PSNR with low computation amount.

Let us consider the monochrome 3-D image $x(u,v,t)$ where u and v are the 2-D spatial axes and t is the time axis. When the current pixel location is (u,v,t), a 11-point window, $W(u,v,t)$, is defined as follows:

$$\begin{aligned} W(u,v,t) = \{ & x(u-1,v-1,t), x(u,v-1,t), \\ & x(u+1,v-1,t),\ x(u-1,v,t),\ x(u,v,t), \\ & x(u+1,v,t),\ x(u-1,v+1,t), x(u,v+1,t), \\ & x(u+1,v+1,t), x(u,v,t+1), y(u,v,t-1)\}. \qquad (2) \end{aligned}$$

As shown in Eq. (2), the window, $W(u,v,t)$, includes a 3×3 window centered at the current pixel of the current frame and the current pixel's corresponding pixels in the previous and the next frames, as shown in Fig. 4. Since the window includes a pixel in the next frame, the algorithm makes one-frame delay. In the previous frame, the element $y(u,v,t-1)$ is the restored output of the previous frame, instead of the original input data, such that $y(u,v,t-1) = \Psi[W(u,v,t-1)]$, where $\Psi[\cdot]$ is the proposed filtering operation. Ten elements of the window, excluding the current pixel $x(u,v,t)$, are

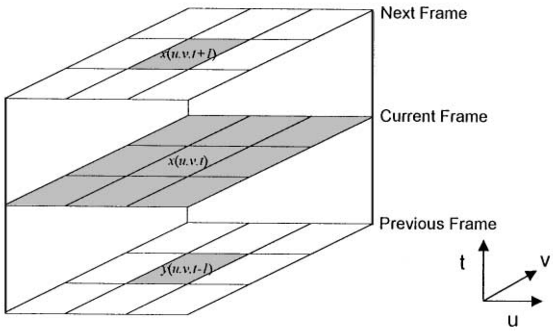

Fig. 4. The elements of the 11-point window $W(u,v,t)$.

rearranged in ascending order [1] as

$$R(u,v,t) = \{r_1(u,v,t), r_2(u,v,t), \ldots, r_{10}(u,v,t)\}, \qquad (3)$$

where $r_1(u,v,t), r_2(u,v,t), \ldots, r_{10}(u,v,t)$ are the elements of $W(u,v,t)$ except $x(u,v,t)$ [3,5]. The rank-ordered mean (ROM) is defined as

$$m(u,v,t) = \frac{r_5(u,v,t) + r_6(u,v,t)}{2}. \qquad (4)$$

Note that the ROM nearly corresponds to the definition of a median filter for a window of even length [1].

There are two nonlinear rank filters in the block diagram shown in Fig. 3. The *nonlinear rank filter-low* is applied when the amount of impulse noise is low, whereas the *nonlinear rank filter-high* is applied to the images which are highly corrupted by impulse noise. One of these two filters is selected based on the estimated number of corrupted pixels. Each processing block in Fig. 3 is described in the following subsections.

3.1. 1-D/3-D switch

In Fig. 3, the 1-D/3-D *switch* ($S2$) selects either the outputs of the *noise rate switch*, $x_m(u,v,t)$, or the original pixel data, $x(u,v,t)$, according to the decision of the *compute 3-D state block*. This block requires three data, such as $y(u,v,t-1)$, $x(u,v,t)$ and $x(u,v,t+1)$. The $y(u,v,t-1)$ is the restored output of the previous frame, and $x(u,v,t+1)$ is the original input data of the next frame. The *backward difference* is defined as the difference between the restored output, $y(u,v,t-1)$, of the previous frame and the original pixel value $x(u,v,t)$ of the current frame, whereas the *forward difference* is the difference between the current frame $x(u,v,t)$ and the next frame $x(u,v,t+1)$. If both the *backward difference* and the *forward difference* are smaller than a given threshold value, the 1-D/3-D *switch* selects $x(u,v,t)$ as the output. If the 1-D/3-D *switch* selects $x(u,v,t)$, the number of computations can be reduced because it is not necessary to compute $x_h(u,v,t)$, $x_l(u,v,t)$ and $x_m(u,v,t)$.

In order to decide the optimal threshold value for 1-D/3-D *switch*, the PSNR and the number of computations are analyzed with respect to various threshold values for the four above-mentioned image sequences which are corrupted by impulse noise. Fig. 5 shows the PSNR and the total number of computations for restoration of these four image sequences corrupted by the impulse noise. As shown in Fig. 5, the threshold of 10 is the optimum value for high PSNR.

3.2. Noise rate switch

In Fig. 3, the *noise rate switch* ($S1$) is controlled by probability of the corrupted pixels. When processing the current frame, the probability of the corrupted pixels in the previous frame is required. In this paper, it is assumed that the impulse noise ratio does not abruptly change in the image

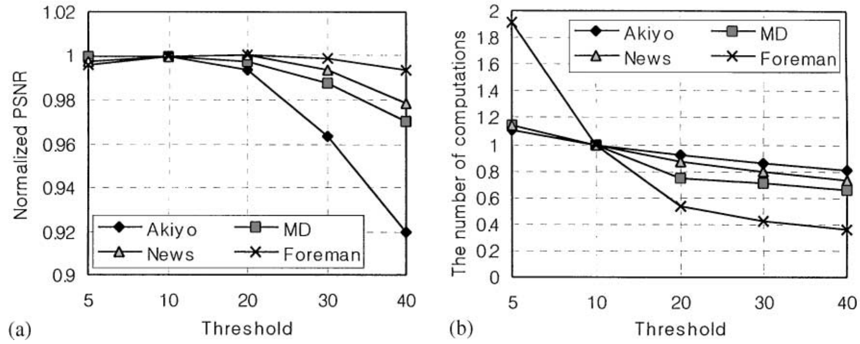

Fig. 5. The PSNR and the number of computations for the various threshold values of the 1-D/3-D switch. The vertical axes are values normalized on the bases of the PSNR and the number of computations at the threshold of 10: (a) PSNR and (b) the number of computations.

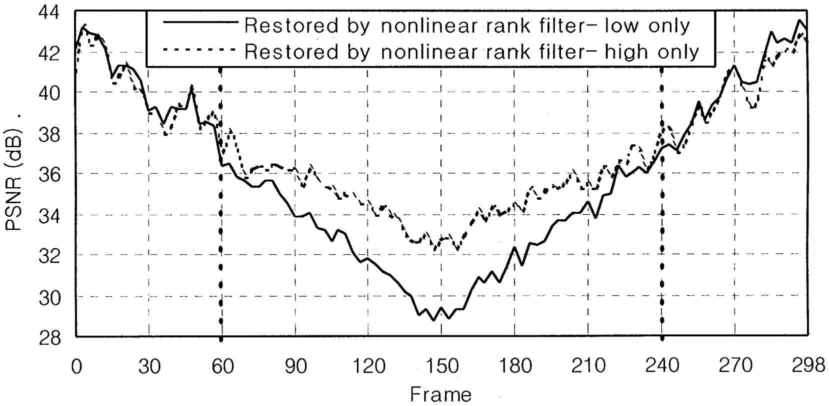

Fig. 6. The PSNR of a restored Akiyo image sequence when the *noise rate switch* selects only $x_l(u,v,t)$ or $x_h(u,v,t)$.

sequence. Therefore, the impulse noise ratio of the current frame can be estimated from that of the previous frame. The proposed algorithm detects the corrupted pixels, replaces them with the ROM, and counts the number of corrupted pixels to control the *noise rate switch*. Using the number of corrupted pixels in the previous frame, the proposed algorithm determines the *noise rate switch* ($S1$) position for restoration of the current frame.

When the impulse noise ratio is larger than 12%, the noise rate switch selects the output of the *nonlinear rank filter-high*, $x_h(u,v,t)$. The threshold of 12% was experimentally obtained. Fig. 6 shows the PSNR of the restored image of Akiyo sequence, which had been corrupted by the impulse noise shown in Fig. 1. In Fig. 6, the vertical dotted lines at frames 60 and 240 are the boundaries of the 12% noise ratio. The image frames from 60 to 240 are highly corrupted with more than 12% noise ratio, so the image frames are restored by the *nonlinear rank filter-high*, whose PSNR is higher than the PSNR from the *nonlinear rank filter-low*, as shown in Fig. 6.

3.3. Nonlinear rank filter-low

When the impulse noise ratio of the previous frame is less than the given threshold value, which is calculated from the estimated number of corrupted pixels, the *noise rate switch* selects the output of the *nonlinear rank filter-low*, which is defined as

$$x_l(u,v,t) = \alpha x(u,v,t) + (1-\alpha)m(u,v,t), \tag{5}$$

where $m(u,v,t)$ is the ROM and α is 0 or 1, i.e. the *nonlinear rank filter-low* selects one of the current pixel value and the ROM as the filter output. In Eq. (5), the coefficient α is determined by the probability of impulse noise at (u,v,t). If it is highly probable that the pixel value at (u,v,t) is corrupted by the impulse noise, the nonlinear filter selects the ROM, i.e. $\alpha = 0$.

In order to define the coefficient α, the rank-ordered differences are defined as

$$d_k(u,v,t) = \begin{cases} r_k(u,v,t) - x(u,v,t) & \text{for } x(u,v,t) \leqslant m(u,v,t), \\ x(u,v,t) - r_{11-k}(u,v,t) & \text{for } x(u,v,t) > m(u,v,t) \end{cases} \tag{6}$$

for $k = 1,\ldots,5$. The rank-ordered differences provide information about the likelihood of corruption at the current pixel. The rank-order differences are compared with the corresponding threshold values which are experimentally determined [1,2]. The coefficient α is set to 0 if any of following inequalities are true:

$$d_k(u,v,t) > \mathrm{TL}_k, \quad \text{where } k = 1,\ldots,5, \tag{7}$$

where the TL_k are the threshold values and $\mathrm{TL}_1 \leqslant \mathrm{TL}_2 \leqslant \mathrm{TL}_3 \leqslant \mathrm{TL}_4 \leqslant \mathrm{TL}_5$. In this case, the pixel value at (u,v,t) is considered to be corrupted by impulse noise so that the output of the *nonlinear rank filter-low* is $m(u,v,t)$. On the other hand, if Eq. (7) is not true for all k, the pixel value $x(u,v,t)$ is

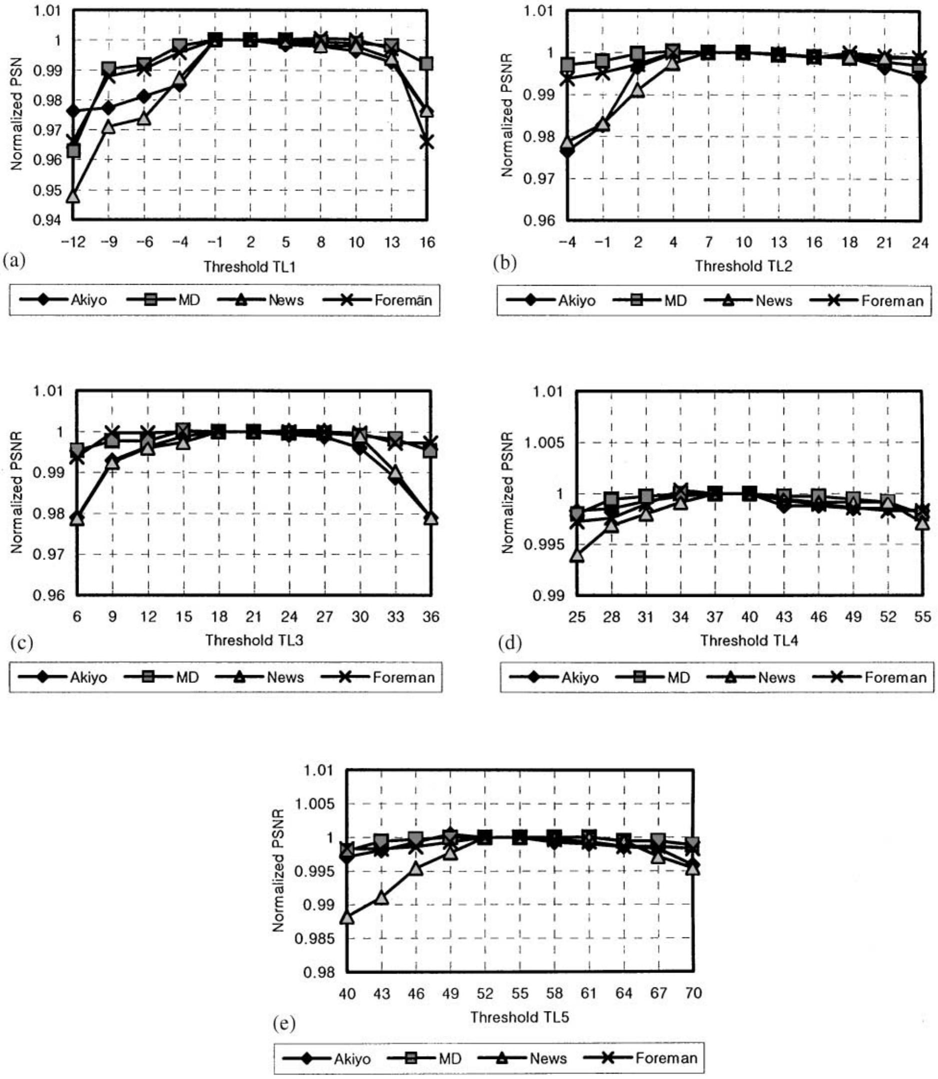

Fig. 7. The normalized PSNR for various threshold values: (a) threshold TL_1 (when $TL_2 = 10$, $TL_3 = 18$, $TL_4 = 40$ and $TL_5 = 55$), (b) threshold TL_2 (when $TL_1 = 2$, $TL_3 = 18$, $TL_4 = 40$ and $TL_5 = 55$), (c) threshold TL_3 (when $TL_1 = 2$, $TL_2 = 10$, $TL_4 = 40$ and $TL_5 = 55$), (d) threshold TL_4 (when $TL_1 = 2$, $TL_2 = 10$, $TL_3 = 18$ and $TL_5 = 55$) and (e) threshold TL_5 (when $TL_1 = 2$, $TL_2 = 10$, $TL_3 = 18$ and $TL_4 = 40$). The vertical axis is the normalized PSNR, which is normalized with the value of the PSNR at the optimal threshold values of $TL_1 = 2$, $TL_2 = 10$, $TL_3 = 18$, $TL_4 = 40$ and $TL_5 = 55$.

the original value which is not corrupted by impulse noise.

In order to decide the threshold values in Eq. (7), the PSNR of the restored image sequence is analyzed with respect to the threshold values of TL_1, TL_2, TL_3, TL_4 and TL_5. Fig. 7 shows the average PSNR of the restored image sequence with respect to the various threshold values. Using these results, the optimal threshold values were selected as $TL_1 = 2$, $TL_2 = 10$, $TL_3 = 18$, $TL_4 = 40$ and $TL_5 = 55$. In Fig. 7, the vertical axis is the normalized PSNR with respect to the value of the PSNR at the optimal threshold value. As shown in Fig. 7, the threshold values are not so sensitive to characteristics of image sequences. Therefore, the threshold values determined in the paper can be applied to other image sequences with a good performance.

3.4. *Nonlinear rank filter-high*

When the impulse noise ratio of the previous frame is higher than the given threshold value, the *noise rate switch* selects the output of the *nonlinear rank filter-high*. Because this filter is selected for highly corrupted images, it is expected that the corrupted pixels exist in the 3-D window $W(u,v,t)$. Since the maximum- and minimum-value elements in the 3-D window are most likely to be pixels corrupted by the impulse noise, they are discarded when computing the rank-ordered differences and their corresponding threshold values.

Since the maximum and minimum values are discarded from the 3-D window $W(u,v,t)$, $r_1(u,v,v)$ and $r_{10}(u,v,t)$ are removed from Eq. (3). Therefore, $d_1(u,v,t)$ is not defined as in Eq. (7), and the inequalities of Eq. (7) are replaced with the equation

$$d_k(u,v,t) > \mathrm{TH}_k \quad \text{where } k = 2,\ldots,5, \tag{8}$$

where the TH_k are threshold values experimentally determined and $\mathrm{TH}_2 \leqslant \mathrm{TH}_3 \leqslant \mathrm{TH}_4 \leqslant \mathrm{TH}_5$. The output of the *nonlinear rank filter-high* is defined as

$$x_m(u,v,t) = \beta x(u,v,t) + (1-\beta)m(u,v,t), \tag{9}$$

where $m(u,v,t)$ is the ROM and β is 0 or 1, i.e., the *nonlinear filter-high* selects one of the current pixel value and the ROM as the filter output.

In order to improve the PSNR of a highly corrupted image sequence, two *nonlinear rank filter-high* operations with different threshold values are cascaded. In this cascade filtering, the first *nonlinear rank filter-high* is applied to the whole frame of the image, then the second *nonlinear rank filter-high* is applied to the result image of the first filtering. The optimal threshold values are defined experimentally by the same procedure as used for the *nonlinear rank filter-low*. The threshold values for the *nonlinear rank filter-high*-1 are $\mathrm{TH}_2 = 2$, $\mathrm{TH}_3 = 10$, $\mathrm{TH}_4 = 30$ and $\mathrm{TH}_5 = 40$, whereas those for the *nonlinear rank filter-high*-2 are $\mathrm{TH}_2 = 8, \mathrm{TH}_3 = 20, \mathrm{TH}_4 = 40$ and $\mathrm{TH}_5 = 50$.

4. Recursive implementation

In Section 3.2, we explained the *nonlinear rank filter-high* for highly corrupted image. In general, recursive implementations of the *nonlinear rank filter-high* have good results for the highly corrupted image sequence. Recursive implementations also require smaller memory space than nonrecursive implementation. The 11-point window, $W(u,v,t)$, is redefined for recursive implementation as follows:

$$\begin{aligned} W(u,v,t) = \{&y(u-1,v-1,t), y(u,v-1,t),\\ &y(u+1,v-1,t), y(u-1,v,t),\ x(u,v,t),\\ &x(u+1,v,t),\ x(u-1,v+1,t), x(u,v+1,t),\\ &x(u+1,v+1,t), x(u,v,t+1), y(u,v,t-1)\}. \end{aligned} \tag{10}$$

Table 1 shows the PSNR of the nonrecursive and the recursive implementations for the corrupted Akiyo image sequence. According to the PSNR result in Table 1, the image corrupted by less than 20% noise has lower PSNR improvement from the recursive filtering than those from the nonrecursive filtering. Because the recursive filtering can replace an original pixel value with the neighborhood pixel value, the restored image from the recursive filtering has low PSNR improvement for the corrupted image with small impulse noise.

5. Simulation results

In this section, the algorithm described in the previous section is evaluated and compared with the conventional nonlinear impulse noise removal

Table 1
Comparison of PSNR between nonrecursive and recursive implementations of *nonlinear rank filter-high* for the Akiyo sequence

Noise ratio	Nonrecursive	Recursive
1%	43.08	42.89
5%	41.03	40.58
10%	38.53	38.36
20%	35.37	35.39
30%	32.15	32.58
40%	28.65	30.12

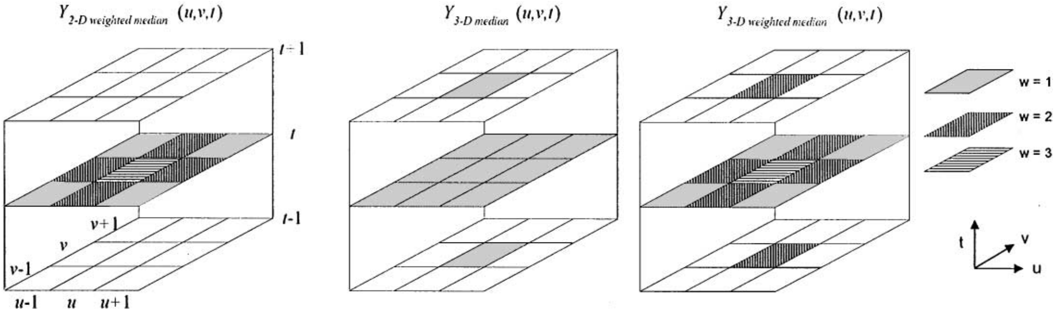
$Y_{2\text{-}D\ weighted\ median}(u,v,t)$
$Y_{3\text{-}D\ median}(u,v,t)$
$Y_{3\text{-}D\ weighted\ median}(u,v,t)$
t+1
t
t-1
v+1
v
v-1
u-1
u
u+1
w = 1
w = 2
w = 3
t
v
u

Fig. 8. The elements and weighted values for the 2-D 3 × 3 weighted median filter, the 3-D median filter, and the 3-D weighted median filter.

techniques. The conventional techniques are 2-D 3 × 3 median filtering, 3-D median filtering, 2-D 3 × 3 weighted median filtering [9], 2-D two-state median filtering [1] and 3-D weighted median filtering [2,9]. Fig. 8 shows the elements of the 2-D weighted median filter, the 3-D median filter, and the 3-D weighted median filter, and their weighted values [9,11]. In this simulation, the impulse noise was uniformly distributed between 0 and 255.

The PSNR of tth frame is defined as

$$\mathrm{PSNR}[t] = 10\log_{10}\left(\frac{\sum_u\sum_v 255^2}{\sum_u\sum_v (y(u,v,t) - v(u,v,t))^2}\right), \tag{11}$$

where $y(u,v,t)$ and $v(u,v,t)$ are the restored image sequence and the original noise-free image sequence, respectively. All image data have 8-bit resolution.

5.1. Experiment 1

In order to compare the PSNR and the number of computations for each filtering technique, 30 frames of an Akiyo monochrome image sequence which had been corrupted by the impulse noise were used. Each frame has a spatial resolution of 176 × 144 pixels. The number of computations is the total number of additions and comparison operations for ordering during the restoration of the image sequence. Simulations were performed for the Akiyo sequence corrupted by the impulse noise with the noise ratios of 1%, 5%, 10%, 20% and 30%.

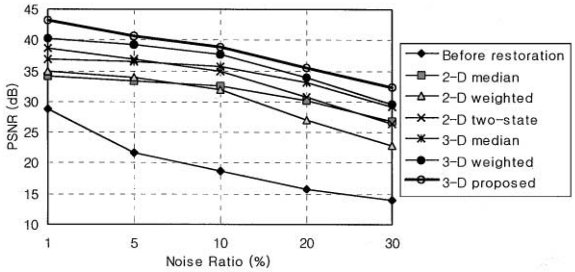

Fig. 9. The average PSNR of 30 frames of an Akiyo sequence which had been corrupted with various values of impulse noise.

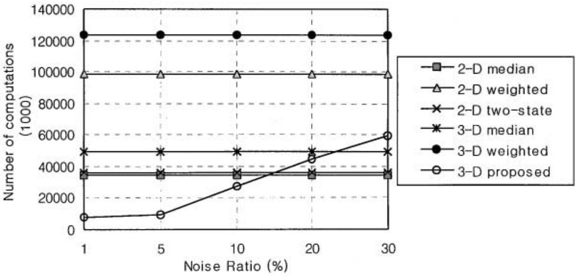

Fig. 10. The number of computations for 30 frames of an Akiyo sequence.

Fig. 9 shows that the proposed algorithm had the best restoration performance with respect to the PSNR. In Fig. 10, the number of computations in the proposed algorithm is greater than that of the 2-D algorithms for high impulse noise ratio. However, the proposed algorithm requires the lowest number of computations among the 3-D algorithms, and lower number of computations than even 2-D algorithms for low impulse noise ratio.

Fig. 11 shows the 30th-frame image of Akiyo sequence, its corrupted images with various noise ratios and their restored images from the proposed restoration algorithm.

5.2. Experiment 2

In this experiment, the PSNR was analyzed for each frame having a different impulse noise ratio.

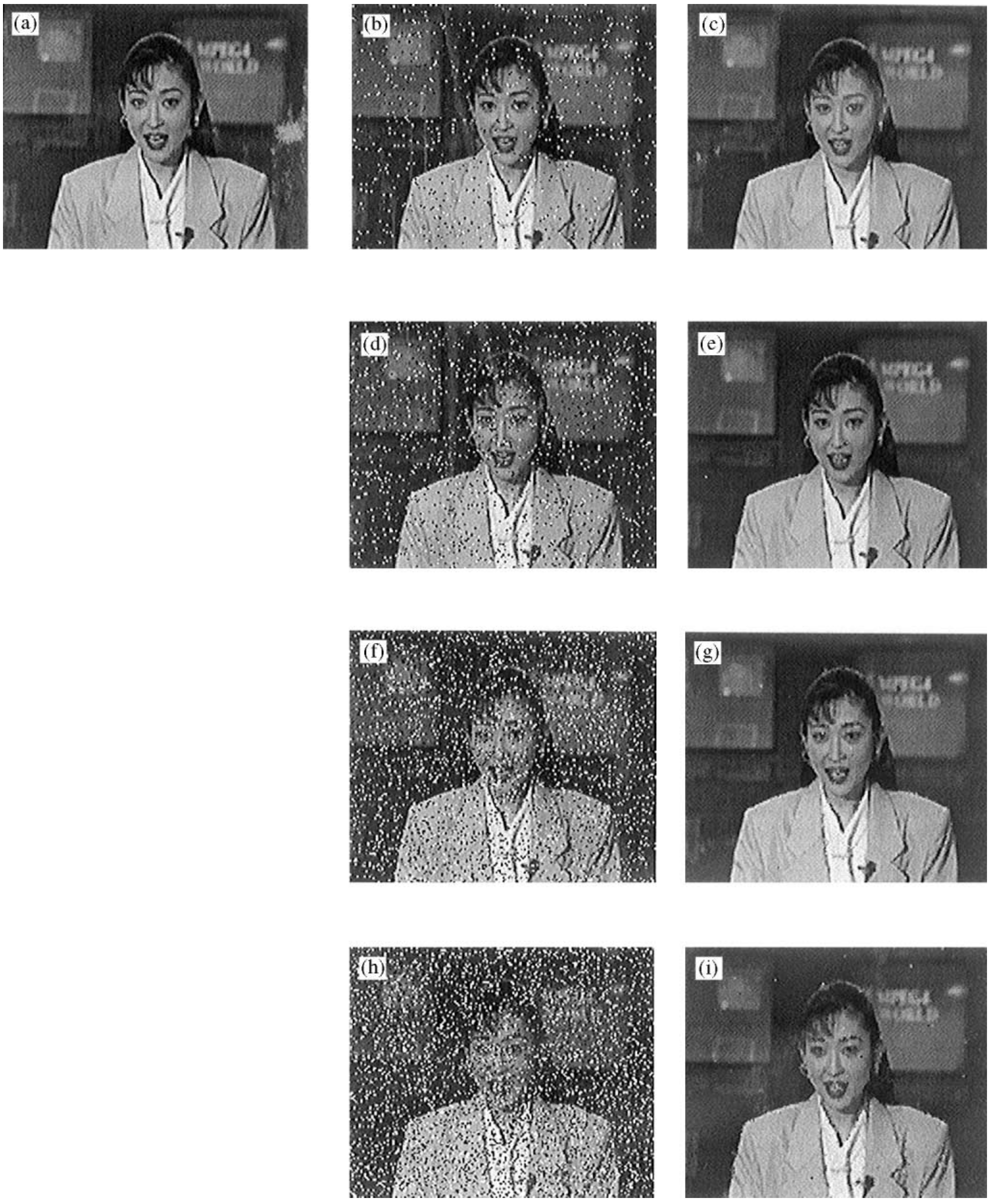

Fig. 11. Example images corrupted by various noise ratios, and their restored images from the proposed filtering method; (a) an original 30-th frame image of Akiyo sequence, (b) corrupted image by impulse noise with noise ratio of 5%, (c) restored image of (b), (d) corrupted image with noise ratio of 10%, (e) restored image of (d), (f) corrupted image with noise ratio of 20%, (g) restored image of (f), (h) corrupted image with noise ratio of 30%, and (i) restored image of (h).

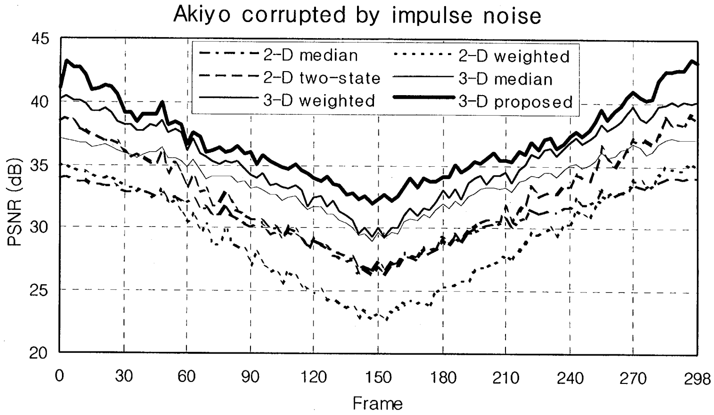

Fig. 12. The PSNR of each image frame of the Akiyo sequence corrupted by the impulse noise shown in Fig. 1.

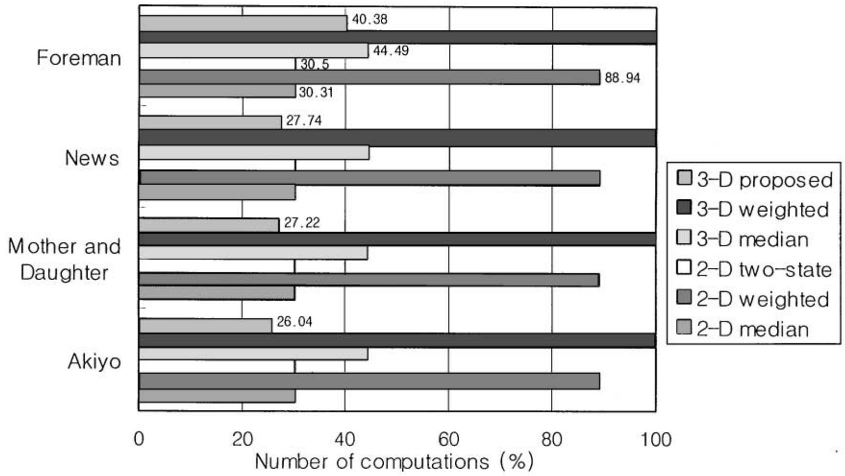

Fig. 13. The number of computations for each image sequence. The number of computations is given as a percentage of the number of computations for 3-D weighted median filtering.

The impulse noise ratio of each frame varied along the time from 0 to 30%, as shown in Fig. 1. The impulse noise was also uniformly distributed from 0 to 255. Fig. 12 compares the PSNR results for the Akiyo sequence. The 3-D impulse noise removal algorithms are generally better than the 2-D algorithms. Also, the proposed algorithm gives a good restoration performance for various image sequences over a wide range of the impulse noise ratio. The experiment results from the other image sequences show the similar results to that from the Akiyo sequence.

Fig. 13 shows the number of computations as percentage of the number of computations for 3-D weighted median filtering for the four image sequences. The number of computations in the proposed algorithm is smaller than those of any other algorithms for the Akiyo, the Mother and Daughter, and the News image sequences. However, the Foreman sequence requires a larger computing for the proposed method than those for the 2-D median and 2-D two-state filtering because there is much motion in the Foreman sequence. The large motion in the image sequence generates a large

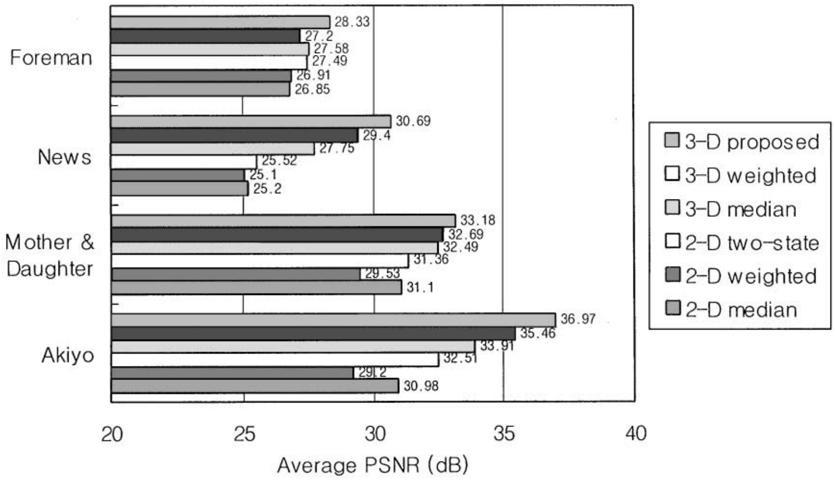

Fig. 14. The average PSNR of various algorithms.

difference between two consecutive frames, thereby making the 1-D/3-D *switch* frequently select $x_m(u, v, t)$ instead of $x(u, v, t)$. Therefore, the number of computations increases in order to compute $x_h(u, v, t)$, $x_l(u, v, t)$ and $x_m(u, v, t)$. Fig. 14 compares the average PSNR results for 300 frames of the four sequences. This figure clearly shows that the PSNR of the proposed algorithm is the highest among those of the conventional nonlinear filtering methods.

6. Conclusions

A new adaptive 3-D median filtering method was proposed for the removal of impulse noise. The proposed method improved the image quality and reduced computing time in comparison with the conventional nonlinear filtering methods. In order to obtain a high performance in image restoration, several threshold values were defined experimentally. Four image sequences, such as the Akiyo, the Mother and the Daughter, the News, and the Foreman, were used to compare the proposed method with the conventional restoration methods for impulse noise. The PSNR and the number of computations were the figures of merit for this comparison study.

In our simulations, the PSNR of the proposed algorithm was better than that of any other 2-D or 3-D impulse noise removal algorithms. The number of computations in the proposed algorithm was very small in comparison with those of the other algorithms. In particular, the number of computations was extremely small for an image frame corrupted with a small impulse noise ratio. For example, in the simulation for an Akiyo sequence which had been corrupted by 1% impulse noise, the number of computations for the proposed algorithm was about 22% of that for the general 2-D median filtering algorithm.

References

[1] E. Abreu, M. Lightstone, S.K. Mitra, K. Arakawa, A new efficient approach for the removal of impulse noise from highly corrupted images, IEEE Trans. Image Process. 5 (6) (June 1996) 1012–1025.

[2] E. Abreu, S.K. Mitra, A signal-dependent rank ordered mean filter – a new approach for removal of impulses from highly corrupted images, in: Proceedings of the Nit. Conference on Acoustic Speech Signal Processing, Detroit, MI, May 1995, Vol. 4, pp. 2371–2374.

[3] M. Lightstone, E. Abreu, S.K. Mitra, K. Arakawa, State conditioned rank ordered filtering for removing impulse noise in images, in: Proceedings of the IEEE International Symposium on Circuit Systems, Seattle, May 1995, Vol. II, pp. 957–960.

[4] J.S. Lim, Two-Dimensional Signal and Image Processing, Prentice-Hall International, Englewood Cliff, NJ, 1990.

[5] S.K. Mitra, T.H. Yu, A new nonlinear algorithm for the removal of impulse noise from highly corrupted images, in: Proceedings of the IEEE International Symposium Circuit Systems, London, May 1994, Vol. 3, pp. 268–275.

[6] S.K. Mitra, T.H. Yu, R. Ali, Efficient detail preserving method of impulsive noise removal from highly corrupted images, SPIE Proc. Image Video Process. 2182 (1994) 43–48.

[7] A. Papoulis, Probability, Random Variables, and Stochastic Processes, 3rd Edition, McGraw-Hill, New York, 1991.

[8] I. Pitas, A.N. Venetsanopoulos, Nonlinear Digial Filters, Kluwer Academic Publishers, Massachusetts, 1990.

[9] M.I. Sezan, R.L. Lagendijk, Motion Analysis and Image Sequence Processing, Kluwer Academic Publishers, Massachusetts, 1993.

[10] Z. Wang, D. Zhang, Progressive switching median filter for the removal of impulse noise from highly corrupted images, IEEE Trans. Circuits Systems-II 46 (1999) 78–80.

[11] H. Zhou, B. Zeng, Y. Neuvo, Weighted FIR median hybrid filters for image processing, in: Proceedings of the IEEE International Symposium Circuits Systems, Shenzhen, Vol. 2, China, June 1991, pp. 793–796.